The evolution of vortices in vertical shear. I: Initially barotropic vortices

By SARAH C. JONES*

Universität München, Germany

SUMMARY

The behaviour of initially-barotropic vortices in vertically-sheared environmental flows is investigated. The strength and structure of the vortices used are representative of tropical cyclones. The calculations are performed using a primitive-equation numerical model on an f-plane. It is found that the initial response of the vortex to the vertical shear is to tilt in the plane of the shear. As soon as a tilt is established, the upper- and lower-level centres begin to rotate cyclonically about the mid-level centre. This rotation can be understood in terms of upper- and lower-level potential-vorticity anomalies which are displaced in the horizontal relative to one another. The flow associated with the vertical projection of each anomaly advects the other anomaly, leading to the observed cyclonic rotation. The rotation rate decreases with time, so that the direction of tilt becomes constant, but the magnitude of the tilt continues to increase. We argue that the observed rotation acts to oppose the destructive action of the vertical shear on the vortex, even in the absence of diabatic processes.

The role of the vertical circulation is considered in detail. It is shown that the vertical circulation develops in a manner which is consistent with the model flow remaining balanced. It is found that the mesoscale nature of the vertical circulation leads to a distortion of the axisymmetric vortex. This results in the inner core having a smaller vertical tilt than the outer region. The vertical circulation does not act on a large enough scale to explain why the vortex is not destroyed by the vertical shear.

The behaviour of the vortex is found to depend on various parameters. Results are presented where the vertical shear, the strength and size of the vortex, the Coriolis parameter, and the static stability are varied. With the exception of the vertical shear, altering any of these parameters alters the vertical penetration of a potential-vorticity anomaly. The results show that increasing the penetration depth leads to an increase in the rotation rate of the upper- and lower-level vortex centres about the mid-level centre, and to a reduction in the magnitude of the vertical tilt.

KEYWORDS: Tropical cyclones   Vertical shear   Vertical circulation   Vortices

1. Introduction

Idealized studies aimed at understanding tropical cyclone motion have to a large extent concentrated on the barotropic problem. More recently, interest has focused on the inclusion of baroclinic effects, particularly on the role of vertical shear. The results from several numerical experiments have shown that the motion of hurricane-like vortices may be either to the left or to the right of the vertical shear. Madala and Piacsek (1975) found that a vortex moved further to the north on a beta-plane under the influence of easterly vertical shear, than in a calculation without any environmental flow. Shapiro (1992) and Wang *et al.* (1993) found motion to the right of the vertical shear also. In contrast, Wu and Emanuel (1993) and Flatau *et al.* (1994) present results where the motion is to the left of the vertical shear.

Several of the above authors have elucidated mechanisms which contribute to the behaviour of such vortices. One of these mechanisms is analogous to an effect which has been studied in detail using barotropic models. In the barotropic case the motion of a vortex can be attributed to advection by the flow associated with wavenumber-one asymmetries in the relative vorticity (Chan and Williams 1987; Fiorino and Elsberry 1989; Shapiro and Ooyama 1990; Smith *et al.* 1990). One of the primary reasons for the development of such asymmetries on the beta-plane is advection of planetary vorticity by the vortex flow. In a baroclinic fluid with a horizontal potential-vorticity gradient the advection of potential vorticity by the vortex flow leads to a wavenumber-one asymmetry in the potential-vorticity field. The flow across the vortex centre associated with this potential-vorticity anomaly

---

* Corresponding address: Meteorologisches Institut, Universität of München, Theresienstr. 37, D-80333 München, Germany.

can contribute to the vortex motion in the same way as that associated with the relative-vorticity anomalies in the barotropic case. This mechanism was demonstrated by Shapiro (1992) using a three-layer model in isentropic coordinates. The presence of an upper-level westerly jet led to a southward potential-vorticity gradient in the middle layer, which resulted in the vortex moving towards the south-east. The sign of the potential-vorticity gradient depends on the curvature of the vertical profile of the environmental wind. Thus the direction of motion cannot be related unambiguously to the direction of the vertical-shear vector. Flatau et al. (1994) present results where westerly shear is accompanied by a northwards potential-vorticity gradient and the motion of the vortex has a northwards component.

A second mechanism was proposed by Wu and Emanuel (1993). This involves the differential advection of the cyclonic vortex and the upper-level anticyclonic circulation by the vertical shear. In this scenario the downward penetrating circulation associated with the anticyclonic potential-vorticity anomaly advects the cyclonic vortex, leading to motion to the left of the vertical-shear vector. This mechanism was found to exist in a two-level quasi-geostrophic contour dynamics model, where the cyclonic part of the circulation was represented as a point vortex and the anticyclonic part emanated from a point source of anomalously low potential vorticity collocated with the vortex. This point source was included as a representation of diabatic processes. Flatau et al. (1994) attribute the motion to the left of the vertical shear in their results to this mechanism.

Wang et al. (1993, hereafter WHL) invoke a similar mechanism, but concentrate on the role of the vertical shear in tilting the cyclonic vortex. This leads also to an upper-level potential-vorticity anomaly which is displaced relative to the lower-level vortex, but in this case the upper-level anomaly is cyclonic. The downwards penetrating circulation associated with this anomaly will tend to displace the surface vortex to the right of the shear. WHL cite the mechanism discussed by Shapiro (1992) as a possible contributor to the difference between the tracks in model runs using different vertical structure.

The behaviour of tropical cyclones in vertical shear is not only interesting in terms of the motion. It is well known that too much vertical shear can inhibit tropical cyclone development. It is important, therefore, to consider whether mechanisms exist which oppose the tendency of vertical shear to destroy a vortex. Flatau et al. (1994) and Wang and Li (1992) both refer to the vertical circulation as a means by which a vortex remains vertically coupled, although they do not discuss exactly how the vertical circulation contributes to this vertical coupling. WHL present a mechanism by which the adiabatic divergent circulation could oppose the differential advection by the environmental shear flow. The proposed mechanism relies on the stretching term in the vorticity equation being oriented such that it opposes the vorticity tendency due to advection by the vertical shear flow. They conclude that the adiabatic vertical circulation is important, even in the presence of diabatic processes (Wang and Holland, personal communication).

Studies of the motion of barotropic vortices have emphasised the role played by vorticity anomalies. The natural extension to these ideas of a baroclinic fluid is the study of anomalies of potential vorticity. As discussed by Hoskins et al. (1985), our understanding of atmospheric flows can be enhanced by studying the potential vorticity, both in idealized models and real data. The two important properties of potential vorticity are that it is conserved in the absence of diabatic or frictional processes and that, given a balance condition and appropriate boundary conditions, it can be inverted to obtain the associated wind and mass fields. For weak vortices the quasi-geostrophic approximation can be invoked to provide a balance condition. However, for Rossby numbers such as those found in tropical cyclones, quasi-geostrophic balance cannot be expected to be very accurate. Other possible balance assumptions together with the regimes for which they are valid

are discussed by Gent and McWilliams (1983). One of the balance equations described is the nonlinear balance equation (Charney 1955; Lorenz 1960). McWilliams (1985) showed that this is a valid approximation to the primitive equations for large Rossby number if the aspect ratio and the Froude number are small. Raymond (1992, hereafter RA) derived a set of equations analogous to the semi-geostrophic equations, but using nonlinear balance. These are valid if the divergence is small compared to the vorticity, even for Froude number of the order of unity, providing the flow in question has only small departures from axially-symmetric or slab-symmetric flow. These conditions may well be met in tropical cyclones, if the divergence associated with convection is not too large.

As described above, it has been proposed that several mechanisms play a role in the behaviour of tropical cyclones in vertical shear. However, more work is necessary to understand these mechanisms in detail. We believe that the idealized representation of hurricane-like vortices without the inclusion of diabatic processes can give further insight into these mechanisms, as none of the mechanisms rely on the presence of the diabatic processes inherent in tropical cyclones. In this paper the behaviour of a cyclonic vortex in vertical shear is studied in more detail. The shear is chosen so that there is no horizontal potential-vorticity gradient. The absence of diabatic processes precludes the development of an upper-level anticyclone. Thus it should be possible to isolate the mechanism described as 'vertical coupling' by WHL. The role of the divergent circulation and the development of the vertical tilt are studied in detail also, with references to ideas presented in RA. The numerical experiments described here use a barotropic vortex as initial condition. This is particularly advantageous for studying the development of the thermal perturbation associated with a tilted vortex, as the initial vortex has no thermal structure. A future paper will generalize these results to the case of a baroclinic vortex.

In section 2 the numerical details of the model and initial conditions are given. Sections 3 and 4 describe the results from one particular model run. Section 3 examines the motion of the vortex and the development of the vertical tilt. We propose an alternative mechanism to that of WHL, which acts to oppose the vertical shear. Section 4 considers the development of the vertical circulation and its role in the maintenance of balance. In section 5 results are described from experiments where parameters such as the size and strength of the vortex, the Coriolis parameter and the static stability are varied. Section 6 summarizes and discusses the results presented in the previous sections.

2. NUMERICAL DETAILS

The model used for the numerical simulations is described in Jones and Thorpe (1992). It is a hydrostatic primitive-equation model formulated in Cartesian coordinates, x and y, on an f-plane. The vertical coordinate is a pressure-based height (Hoskins 1971). The prognostic variables are the horizontal wind components, u and v, and the potential temperature, θ. The vertical velocity, w, and the geopotential, ϕ, are diagnosed from the continuity and hydrostatic equations respectively. Periodic lateral boundary conditions are used for the perturbation fields. The vertical velocity is set to zero on the upper and lower boundaries. The model uses the Arakawa 'C' grid (Arakawa and Lamb 1977) in the horizontal. The grid is staggered in the vertical also, with w stored on intermediate levels to the other model variables.

The model is initialized with the Eady basic state (Eady 1949). The vertical shear flow is given by:

$$\overline{U} = U_0 + U_z z$$

where U_0 and U_z are constants. This flow is in thermal wind balance with a stably-stratified temperature field. The static stability N, given by $N^2 = (g/\theta_0)(d\theta/dz)$, is constant, where

TABLE 1.   DETAILS OF THE VARIOUS VORTEX PROFILES

Profile	Eq.:	v_{max} (ms^{-1})	r_{max} (km)	Profile parameters		
Standard	(1)	40	100	$v_0 = 71.521$	$a = 0.3398$	$b = 5.377 \times 10^{-4}$
30 m s^{-1}	(1)	30	100	$v_0 = 53.641$	$a = 0.3398$	$b = 5.377 \times 10^{-4}$
20 m s^{-1}	(1)	20	100	$v_0 = 35.761$	$a = 0.3398$	$b = 5.377 \times 10^{-4}$
Broad	(2)	40	150	$v^* = 84.647$	$\alpha = 0.4549$	$\mu = 0.3747$

θ_0 is a reference potential temperature of 300 K. The standard run described in sections 3 and 4 has $U_0 = 4$ m s^{-1}, $U_z = -4 \times 10^{-4}$s^{-1} and $N^2 = 1.5 \times 10^{-4}$s^{-2}. Calculations are performed for a latitude of $12.5°$N. Since the shear, the static stability, and the Coriolis parameter are constant, this flow has uniform potential vorticity. Some of the results shown later are in the form of perturbation fields, where the background fields detailed above have been subtracted.

An axisymmetric barotropic vortex is superimposed on this initial state. Two vortex profiles are used in the model runs described here. The standard profile is that used by Smith *et al.* (1990). The tangential wind, v_T, is given by:

$$v_T = v_0 \frac{s \left(1 + \frac{5b}{2a}s^4\right)}{(1 + as^2 + bs^6)^2} \qquad (1)$$

where s is the ratio of the radius, r, to the radius of maximum winds, r_{max}, and v_0, a and b are constants. The vortex used in the standard run has a maximum tangential wind (v_{max}), of 40 m s^{-1}. The radius of maximum wind is 100 km and the radius (r_g) of gale force winds ($v_T = 15$ m s^{-1}) is 300 km. The behaviour of weaker vortices, described in section 5, is investigated by reducing v_0 to give a maximum tangential wind of either 30 m s^{-1} or 20 m s^{-1}. The same values of a and b are used to retain the same horizontal structure. The effect of varying the horizontal profile is investigated by specifying the tangential wind as:

$$v_T = v^* \frac{s \exp(-\mu s)}{1 + \alpha s^2} \qquad (2)$$

where v^*, μ and α are chosen to give $v_{max} = 40$ m s^{-1}, $r_{max} = 150$ km and $r_g = 460$ km. The parameters used in both profiles are given in Table 1.

In order to minimize the influence of the periodic lateral boundary conditions it is important that the vortex is localized. Both of the profiles used have the advantage that the tangential wind decays rapidly as $r \to \infty$. However, for the domain sizes used, the tangential velocity at the boundary is small, but not exactly zero. Reducing the velocity to zero over one horizontal grid-length results in a large vorticity gradient, even if the velocity is small. Such a large vorticity gradient can lead to inaccuracies in the calculation. To prevent this occurring the tangential velocity is multiplied by a function, $\varepsilon(r)$, given by:

$$\varepsilon(r) = \begin{cases} \left[1 - \exp\left(-\frac{(r - r_{cut})^2}{r_{wid}^2}\right)\right] & r \leqslant r_{cut} \\ \\ 0 & r > r_{cut} \end{cases}$$

When the value of r_{cut} is large enough this reduces the vorticity gradient smoothly to zero,

TABLE 2. MODEL PARAMETERS FOR THE STANDARD RUN AND THE MODEL RUNS DESCRIBED IN SECTION 5

Track shown in:	Profile	Domain in x (km)	Domain in y (km)	Domain height (km)	r_{cut} (km)	Remarks
Fig. 1	Standard	3840	2880	10	1000	Standard Run; f-plane at 12.5°N, $N^2 = 1.5 \times 10^{-4}\mathrm{s}^{-2}$, $U_0 = 4$ m s^{-1}, $U_z = -4 \times 10^{-4}\mathrm{s}^{-1}$.
Fig. 12(a)	Standard	2880	1920	10	900	As standard run but $U_0 = 6$ m s^{-1}, $U_z = -6 \times 10^{-4}\mathrm{s}^{-1}$.
Fig. 12(b)	Standard	2880	1920	10	900	As standard run but $U_0 = 8$ m s^{-1}, $U_z = -8 \times 10^{-4}\mathrm{s}^{-1}$.
Fig. 13(a)	30 m s^{-1}	2560	1620	10	780	As standard run, apart from vortex strength.
Fig. 13(b)	20 m s^{-1}	2560	1620	10	780	As standard run, apart from vortex strength.
Fig. 14(a)	30 m s^{-1}	2560	1620	10	780	As standard run, except $N^2 = 1 \times 10^{-4}\mathrm{s}^{-2}$ and 30 m s^{-1} vortex.
Fig. 14(b)	30 m s^{-1}	2560	1620	10	780	As standard run, except f-plane at 20°N and 30 m s^{-1} vortex.
Fig. 14(c)	Standard	2560	1920	10	900	As standard run except $f = 0$.
Fig. 15(a)	Broad	4860	3840	10	1900	As standard run except $U_0 = 6$ m s^{-1}, $U_z = -6 \times 10^{-4}\mathrm{s}^{-1}$ and broad profile.
Fig. 15(b)	Standard	2880	2560	14	900	As standard run apart from height of vortex.

without giving any sharp changes in the vorticity gradient. The values of r_{cut} used are given in table 2; r_{wid} was always 100 km.

The vortex is introduced into the model by calculating a stream function, ψ, where $v_T(r) = d\psi/dr$. The stream function is interpolated to the model grid and the velocity components u and v are calculated from it. Hence the initial wind field is non-divergent and the continuity equation is automatically satisfied. Since the vortex is barotropic there is no initial potential-temperature perturbation. No other initialization was found to be necessary.

The representation of an axisymmetric vortex on a Cartesian grid is not exact. A spurious numerical mode with wavenumber four was found to exist in the vertical velocity. It can be shown that this results from the discretization on the Cartesian grid. The amplitude of this mode is not significant if the horizontal grid-length adequately resolves the vortex profile. For a radius of maximum winds of 100 km the profile was found to be well-resolved when a horizontal grid-length of 10 km was used. However, even when the amplitude of the mode is small, its presence leads to enhanced small-scale noise in the divergent part of the flow. In order to control this noise without significantly damping the initial vortex, a second-order diffusion was added to the divergent part of the flow. A sixth-order horizontal diffusion was used on the total wind and temperature fields, with weak second-order diffusion in the vertical. The diffusion terms require extra boundary conditions in the vertical. We use stress-free boundary conditions for perturbation quantities, i.e. $\partial\chi/\partial z = 0$ at $z = 0$, $z = H$, where χ is the perturbation wind or potential temperature. When the diffusion is formulated in this manner and the model initialized with a barotropic vortex, but without vertical shear, the vortex remains stationary and its amplitude alters by less than 0.5 m s^{-1} over 48 hours. The effect of using a stronger damping for the divergent part

of the flow was tested by comparing two simulations which differed only in the magnitude of the divergence damping. It was found that doubling the amount of damping of the divergent part of the flow had no significant effect on the vortex track. A run without vertical diffusion showed that this does not influence the vortex track.

The use of doubly-periodic lateral boundary conditions necessitates using a sufficiently large domain that the results are not influenced by the boundary conditions. Tests were made using various domain sizes to ensure that the boundaries did not influence the results. As expected, the runs with stronger vortices required larger domains than those with weaker vortices. The domain sizes used and other details of the model runs are given in Table 2. The horizontal grid-length was always 10 km, the vertical grid-length 2 km and the time-step 30 seconds.

3.   VORTEX MOTION AND DEVELOPMENT OF THE VERTICAL TILT

This section describes the behaviour of the standard vortex in a uniform vertical shear flow, using parameters given in Table 2. The height of the model domain is 10 km. Hence the environmental flow is 4 m s^{-1} at the lower boundary and zero at the upper boundary. The track followed by the vortex is shown in Fig. 1. In Figs. 1(a) and 1(b) the vortex centre at each model level is defined as the location of the minimum perturbation geopotential. Figure 1(c) shows the same track as Fig. 1(b), but uses the position of maximum potential vorticity to define the centre. The relative merits of these two definitions of the vortex centre are discussed in section 4. Figure 1(a) shows both the motion and the vertical tilt of the vortex at 6 hourly intervals over 96 hours. The overall direction of vortex motion is eastwards. This might be expected, since the vortex is embedded in a westerly environmental flow. We can compare the eastward component of vortex motion at each level with the environmental flow at the same level. At mid-levels, shown by the square, the speed of motion is close to the speed of the environmental flow. At the surface the vortex moves significantly slower than the surface environmental flow. At the top of the model the vortex moves faster than the environmental flow. The vertical tilt of the vortex increases with time, but is much smaller than that which would be implied by simple advection by the basic flow. (This would lead to a separation of 1100 km between the vortex centre at $z = 1$ km and $z = 9$ km after 96 hours.)

The vertical tilt of the vortex shows that the vortex is not simply advected by the environmental shear flow. Figure 1(b) shows the vortex track up to 48 hours, illustrating the behaviour in the early stages of the model run. Here it can be seen that the initial motion of the surface centre has a northwards component, whilst the motion of the upper-level centre has a southwards component. The vortex centre at 5 km moves almost due east, whilst the upper- and lower-level centres rotate cyclonically about it. This rotation results in the surface centre being due north of the upper-level centre at 12 hours. The continued rotation then leads to the surface centre moving towards the south and the upper-level centre moving northwards. The rotation rate decreases with time, so that the direction of tilt remains almost constant over the last 24 hours of the model run (Fig. 1(a)). The magnitude of the vertical tilt increases steadily over the 96 hour period.

The behaviour of the vortex is further illustrated in Fig. 2, which shows horizontal cross-sections of the density-weighted potential vorticity at $z = 1$ km (solid lines) and $z = 9$ km (dashed lines). The density-weighted potential vorticity of the initial vortex does not vary with height. After 6 hours (Fig. 2(a)) a difference can already be seen in the horizontal location of the vortex at upper and lower levels. The orientation of the vertical tilt is NE–SW. At 12 hours (Fig. 2(b)) the tilted vortex has rotated cyclonically so that the tilt is N–S. After 24 hours the vortex at lower levels is located to the west of the vortex
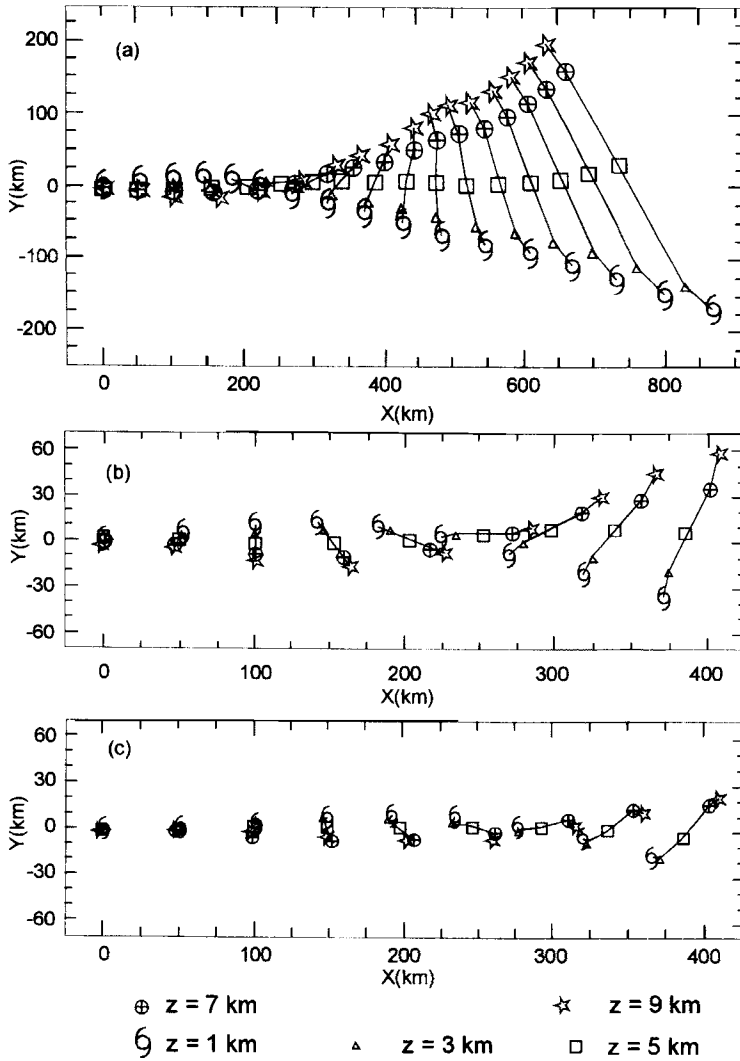
Figure 1.   Vortex track. Symbols show the location of minimum perturbation geopotential at each model level every 6 hours for (a) 96 hours and (b) 48 hours. (c) as (b) but symbols show location of maximum potential vorticity.

at upper levels. This tilt is opposite to that which would be expected from the direction of the vertical shear. The cyclonic rotation continues, as seen in Figs. 2(d), (e), (f). The rotation rate decreases, but the vertical tilt continues to increase so that at 96 hours there is no horizontal overlap between the upper- and lower-level positive potential-vorticity anomalies.

In order to explain the behaviour of the vortex, we consider the initial flow to consist of two identical potential-vorticity anomalies, an upper-level and a lower-level anomaly, with the same horizontal location. As soon as the vertical shear is applied, the lower anomaly is displaced to the east of the upper anomaly. The downward projection of the upper anomaly gives a cyclonic circulation at the surface, which is displaced to the west of the lower anomaly. This flow has a southerly component across the centre of the lower potential-vorticity anomaly, tending to advect the lower anomaly to the north. The reverse
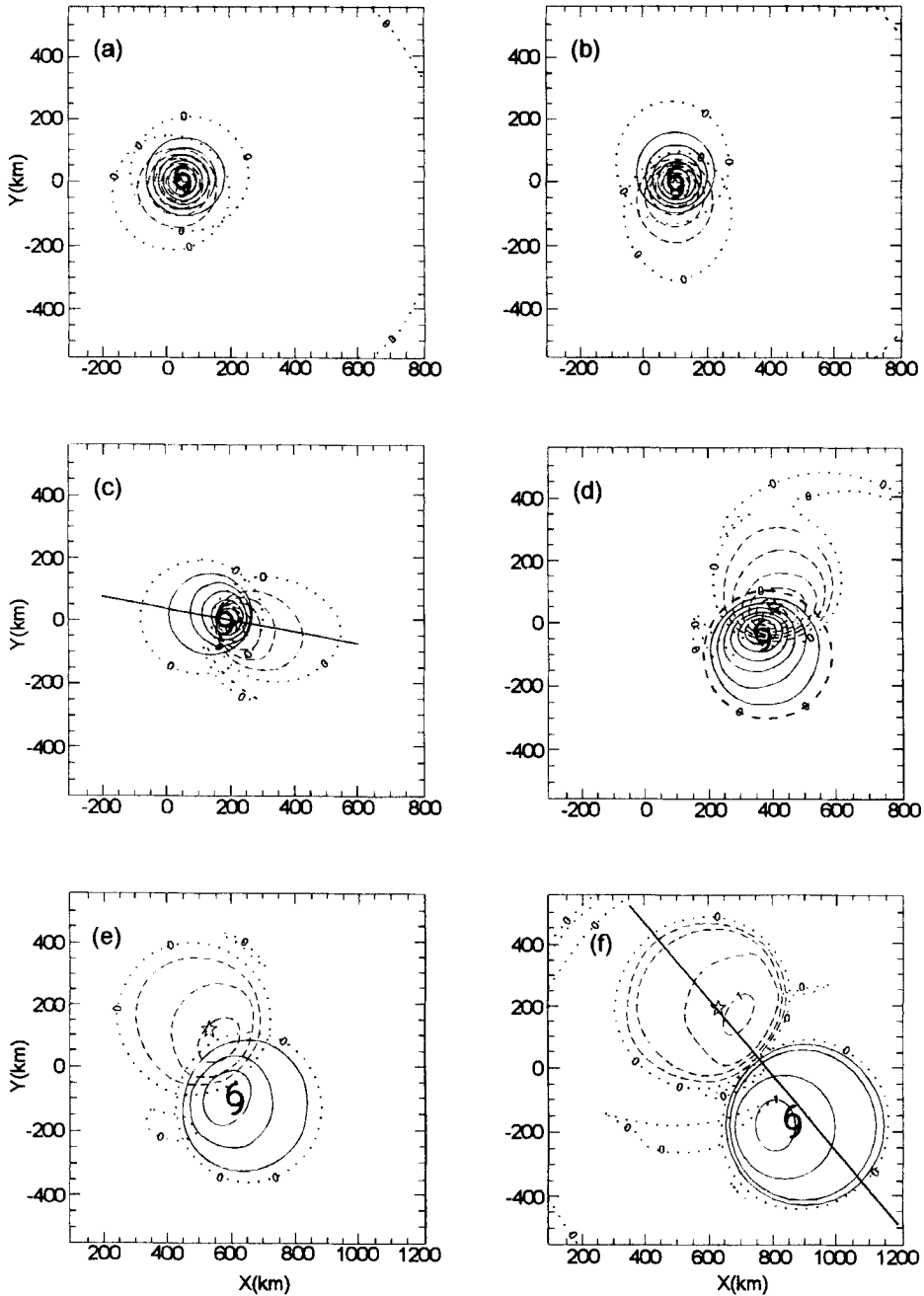
Figure 2. Horizontal cross-sections of the upper and lower level density-weighted potential vorticity fields. The density-weighted potential vorticity of the background flow has been subtracted. The solid contours are for $z = 1$ km, the dashed contours for $z = 9$ km. In both cases the zero line is dotted. The position of minimum perturbation geopotential at $z = 1$ km is marked by a cyclone symbol and that at $z = 9$ km by a star. Only a portion of the model domain is shown. (a) 6 hours, (b) 12 hours, (c) 24 hours. The solid line shows the position of the cross-section in Fig. 6. (d) 48 hours, (e) 72 hours, (f) 96 hours. The position of the cross-section in Fig. 9 is shown. The contour intervals are $1 \times 10^{-6} \text{ m}^{-1}\text{s}^{-1}$ K in (a), (b) and (c); $0.5 \times 10^{-6} \text{ m}^{-1}\text{s}^{-1}$ K in (d) and (e); $0.25 \times 10^{-6} \text{m}^{-1}$ K in (f).

occurs for the upper anomaly, which is advected southwards due to the upward projection of the lower anomaly. The northward displacement of the lower anomaly and southward displacement of the upper anomaly leads to the line joining the centres of the two anomalies no longer lying in the east–west direction. Therefore, the flow across the centre of the lower anomaly due to the downward projection of the upper anomaly has an easterly component. Thus both the upper and lower anomalies continue to rotate about each other in a cyclonic manner.

This description of the rotatory mechanism in terms of two potential-vorticity anomalies is a simplification of what actually happens. In reality, the flow at the surface will be associated with the tilted potential-vorticity anomaly, with contributions from all model levels not just from the highest level. The strength of the interaction will depend on the depth over which the influence of an anomaly extends. For the parameters used here it is not entirely clear how such a penetration depth should be defined. The penetration depth from quasi-geostrophic theory is fL/N, where f is the Coriolis parameter and L is the horizontal length scale of the anomaly. Taking L to be 360 km (the diameter of the positive potential-vorticity anomaly) gives a penetration depth of approximately 930 m. This is too small to account for the interaction described here. Davis (1992) showed that, for the non-linear balance equations, the penetration depth depends on the strength of the anomaly. An alternative expression for the penetration depth of a nearly axisymmetric vortex is $(f_{loc}(f + \zeta))^{1/2}L/N$, where $f_{loc} = f + 2v_T/r$ and ζ is the vertical component of relative vorticity (Hoskins *et al.* 1985; Shapiro and Montgomery 1993). Since the vorticity profile of the vortex is very strongly peaked it is not clear exactly how to apply this formula to such a vortex. If, however, the average relative vorticity and tangential wind within a horizontal radius of 180 km are used, the penetration depth is 14 km. This would allow for significant interaction between the upper- and lower-model levels.

The interaction between an upper- and lower-level potential-vorticity anomaly has been used by previous authors to account for deviations in the vortex track from the direction of the shear vector. Wu and Emanuel (1993) and Flatau *et al.* (1994) attribute a vortex movement to the left of the shear vector to the interaction between the upper-level anticyclone and the cyclonic vortex, which are displaced relative to one another by the vertical shear. WHL explain a movement to the right of the shear vector in terms of the vertical interaction of two cyclonic vortices. The results here show a case where this vertical interaction results in the surface centre being displaced significantly to the left of the shear vector. The direction of motion resulting from this mechanism will depend on a number of factors which are discussed in section 5. Knowledge of the direction of the shear vector alone is not sufficient to determine the direction of motion. It may be misleading to associate motion to the left of the shear with an upper-level anticyclone or motion to the right of the shear with a tilted cyclonic vortex.

The behaviour of the tilted vortex may be compared with the barotropic two-vortex problem. In the barotropic case the two vortices either come closer together and merge, or they move away from each other. Polvani (1991) has studied the analogous problem for a two-layer quasi-geostrophic system. He studies the behaviour of a two-vortex system, with an upper-level and lower-level vortex. Here the analogue of the merger process is alignment. This occurs when the initial centres of two vortices are not horizontally collocated, but the horizontal distance between the two centres decreases with time. Alignment was observed for a certain parameter range. No alignment was observed when the radius of the vortex patches was smaller than the radius of deformation. In the case studied here there is no initial horizontal separation of the upper- and lower-level vortices. The horizontal advection of the vortices by the vertical shear flow acts to increase the horizontal separation. However, there is a significant increase in the separation of the upper- and lower-level vortices in

the N–S direction, which cannot be attributed to the vertical shear. It appears that the vertical shear acts to increase the separation of the two vortices until they are too far apart for alignment to occur. They then move apart in a similar manner to that observed in the barotropic two-vortex problem.

The rotation described above may act to counteract the effect of the vertical shear in two ways. Firstly, if the vortex is displaced northwards at lower levels relative to the position at upper levels, the structure of the flow in the vertical is such that there is an easterly component across the vortex centre at lower levels and a westerly component at upper levels. Thus there is a vertically sheared flow due to the tilt of the vortex. This acts in the opposite direction to the easterly environmental shear, provided the surface vortex centre is to the north of the upper-level vortex centre. When the surface centre is to the south of the upper-level centre this effect would tend to oppose a westerly environmental shear. In the model run described here the surface centre is to the north of the upper-level centre for the first 30 hours, thus the action of the vertical shear is reduced. Secondly, the mutual rotation alters the tilt of the vortex, such that between 12 and 60 hours the vortex near the surface is to the west of the vortex at upper levels. During this time period, advection by the easterly environmental shear flow acts to reduce the tilt of the vortex in the x–z plane rather than increasing it. After 60 hours both the mutual rotation and the environmental shear tend to increase the vertical tilt in the x–z plane.

4. THE ROLE OF THE VERTICAL CIRCULATION

In this section the development of the vertical circulation is described and its role in the maintenance of balance considered. In the early stages of the model run, both the departures from axisymmetry and the divergence are small. Thus the conditions for the semi-balanced equations described by RA are satisfied. Hence the potential vorticity could be inverted to give the associated wind and temperature fields. If the initial potential-vorticity anomaly is tilted by the vertical shear, and the flow remains balanced, a potential-temperature anomaly must develop. One way of achieving the required thermal perturbation in a primitive-equation model is through vertical advection. This has been discussed by Hoskins *et al.* (1985) and RA.

The initial development of the vertical circulation and potential-temperature anomaly is illustrated in Fig. 3, using horizontal cross-sections at $z = 5$ km. The vertical velocity at 30 minutes (Fig. 3(a)) has a wavenumber-one pattern, with ascent to the west and descent to the east of the vortex centre. At this time a weak potential-temperature perturbation can be seen (Fig. 3(b)). This perturbation consists of a warm anomaly in the descent region to the east of the vortex and a cold anomaly in the ascent region to the west of the vortex. These anomalies develop because of vertical advection of the stably-stratified fluid. After 6 hours the relative orientation of the vertical velocity and the potential-temperature perturbation has changed. The pattern of vertical velocity has rotated anticyclonically (Fig. 3(c)), whilst the potential-temperature perturbation has rotated cyclonically, giving a 90° phase shift between the two anomalies. The cyclonic rotation of the potential-temperature anomaly is due to horizontal advection of the anomaly by the vortex flow. Both the vertical circulation and the temperature anomaly have increased in magnitude over the first 6 hours of the model run. There is no evidence of horizontal advection of the environmental potential-temperature field by the vortex flow in Fig. 3. This would produce a thermal anomaly of the opposite sign, with a negative anomaly to the east and a positive anomaly to the west of the vortex. Such an anomaly is seen only in the very early stages of the integration.

The development of the vertical velocity described above can be attributed to three of the mechanisms described by RA. These are illustrated schematically in Fig. 4. The first
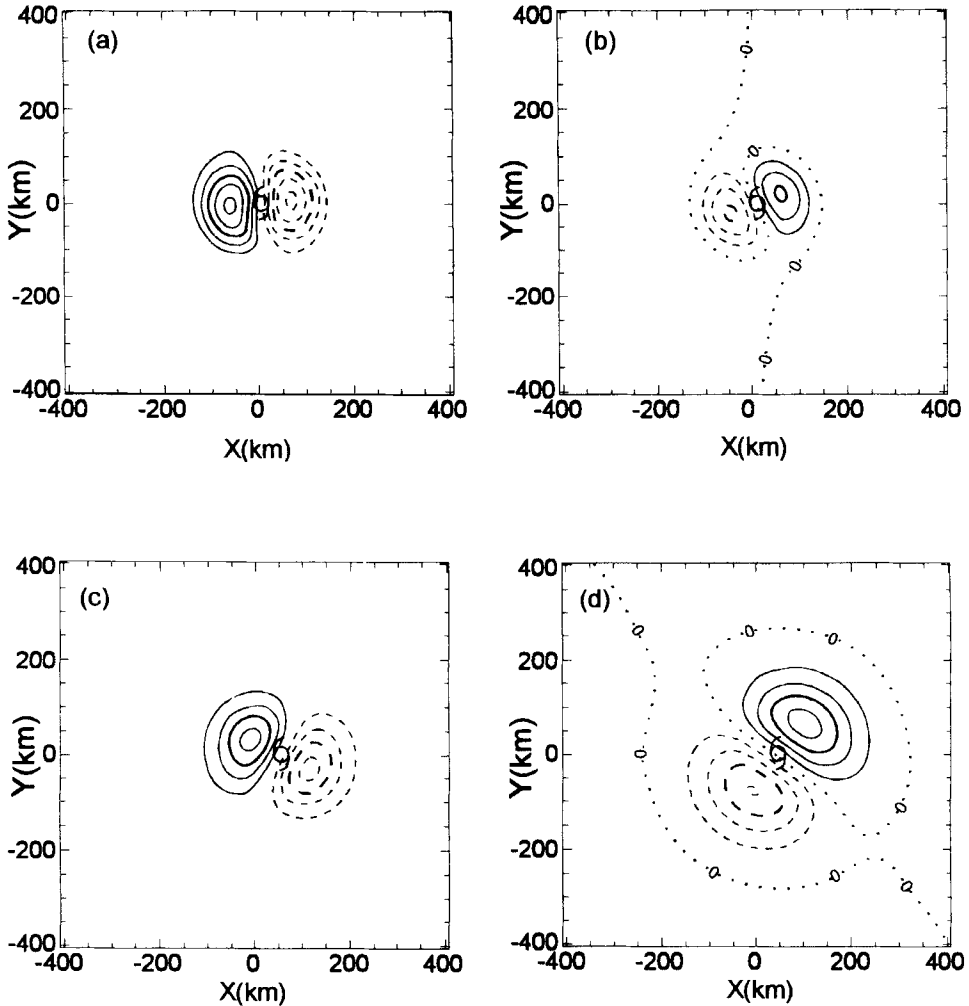
Figure 3.   Horizontal cross-sections showing the development of the vertical circulation and potential-temperature perturbation. (a) Vertical velocity at 30 min, contour interval is 1 cm s^{-1}. (b) Potential-temperature perturbation at 30 min, contour interval is 0.05 K. (c) Vertical velocity at 6 hours, contour interval is 5 cm s^{-1}. (d) Potential-temperature perturbation at 6 hours, contour interval is 0.5 K.

mechanism is associated with the interaction between the vortex flow and the environmental temperature field. Thermal wind balance of the negatively-sheared background flow gives a positive N–S potential temperature gradient, so that the environmental potential-temperature surfaces slope downwards towards the north, as shown in Fig. 4(a). If the cyclonic vortex circulation is along these surfaces, the southerly branch of the circulation would be descending and the northerly branch ascending. This would give rise to the ascent/descent pattern seen in Fig. 3(a). At first glance this appears to be a plausible explanation for the development of the vertical circulation. However, this mechanism cannot account for the potential-temperature anomaly seen in Fig. 3(b). In these calculations there are no diabatic processes which could produce thermal anomalies. Therefore, departures from the initial potential-temperature field, such as seen in Fig. 3, can arise only due to advection. The initial vortex, itself, has no thermal structure, hence temperature anomalies observed early in the model run must arise from advection of the environmental
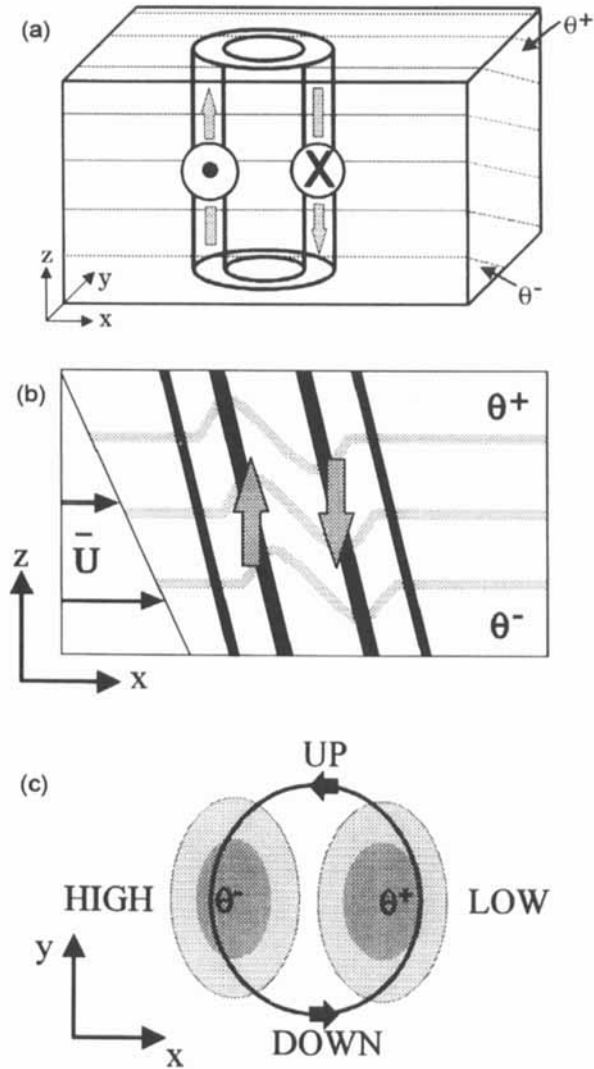
Figure 4.   Schematic of the mechanisms contributing to the vertical circulation. (a) The northward sloping envi-
ronmental potential-temperature field is illustrated by the thin lines. The bold lines indicate the potential-vorticity
anomaly, with associated flow into the page to the east and out of the page to the west of the vortex centre. The
arrows indicate the vertical motion implied if the vortex motion lies along the environmental potential-temperature
surfaces. (b) The potential-vorticity anomaly, indicated by the bold lines, has been tilted due to advection by the
vertical shear flow shown on the left hand side of the diagram. The associated balanced potential-temperature
perturbation, shown by the grey lines, can be achieved by vertical advection, as shown by the large arrows. (c)
A plan view of the potential-temperature perturbation. The shaded region shows a positive potential-temperature
anomaly where the isentropes are lowered and a negative potential-temperature anomaly where they are raised.
The bold circle illustrates the relative motion through the anomaly, which descends as it moves towards the region
of lowered isentropes and ascends as it moves towards the region of raised isentropes.

temperature field by the vortex flow. If the vortex flow lies exactly along the environmental
isentropes, as envisaged in the above mechanism, there will be a vertical velocity but no
temperature advection and therefore no thermal anomaly. The orientation of the potential-
temperature perturbation indicates that the motion must have a steeper slope than that of
the environmental potential-temperature surfaces. The mechanism illustrated in Fig. 4(a)

gives no indication of why this should be the case, and can be at most a partial explanation for the observed vertical circulation.

The second mechanism regards the vertical circulation as a means to achieve the temperature perturbation necessary for balance. RA shows an example of a balanced temperature field associated with a tilted potential-vorticity anomaly, where the isentropes are raised in the direction towards which the vortex tilts and lowered on the other side of the vortex. In the case presented here the advection of potential vorticity by the environmental shear will tilt the anomaly in the direction illustrated by the solid black lines in Fig. 4(b). If the vortex remains balanced a similar isentropic configuration to that shown by RA might be expected. As illustrated in Fig. 4(b) this requires that the balanced isentropes must be raised to the west and lowered to the east of the vortex.

An indication as to why the isentropic structure should have the form shown in Fig. 4(b) can be obtained if we assume that the vertical shear tilts the vortex in the vertical without changing the horizontal wind profile. In this case the location of maximum wind will be tilted also, as illustrated by the thicker black lines in Fig. 4(b). The vortex flow varies with radius such that the tangential wind speed increases to a maximum indicated by the thicker black lines and then decreases. When the vortex is tilted the tangential wind varies in the vertical also. For the direction of tilt shown in Fig. 4(b) the horizontal wind profile results in positive vertical shear between the thicker black lines and negative vertical shear elsewhere. If the vortex were a two-dimensional vortex in thermal wind balance, this vertical shear would be accompanied by a horizontal temperature gradient which is positive between the locations of maximum tangential wind and negative elsewhere. The isentropic surfaces shown in Fig. 4(b) exhibit such a horizontal potential-temperature gradient. For the vortex considered here curvature effects may contribute further to the thermal anomaly. However, since the curvature effects act in the same direction, the potential-temperature structure of the tilted vortex in these calculations is consistent with the above description.

The configuration of isentropes seen in Fig. 4(b) can be achieved by vertical advection of the environmental potential-temperature field. Ascent to the west and descent to the east of the vortex would distort the isentropic surfaces in the observed manner. Hence this mechanism appears to be a candidate for the explanation of the observed circulation. Since the strength of the temperature anomaly required to maintain balance will depend on the size of the vertical tilt, this implies that the strength of the vertical circulation should be related to the magnitude of the vertical tilt. This is observed in the calculations discussed in section 5.

The above two mechanisms account for the vertical circulation seen at the beginning of the model run. Since substantial potential-temperature anomalies develop we infer that the second mechanism makes an important contribution to the circulation. The potential-temperature anomalies alter the potential-temperature field in the vicinity of the vortex, so that a third mechanism must be considered. If the thermal anomaly does not rotate, parcels of air advected by the vortex flow move through the thermal anomaly in a cyclonic manner. A plan view of the deformed isentropes is shown in Fig. 4(c). The path taken by a parcel of air moving through the anomaly is illustrated by the bold circle. Since the flow is adiabatic such a parcel moves along an isentropic surface. As it moves towards the region of lowered isentropes it must descend. As it moves back towards the raised isentropes it ascends. This implies a wavenumber-one pattern of ascent and descent, with a phase shift of 90° to the potential temperature anomaly. However, the thermal anomaly is not stationary, but rotates cyclonically. Thus we must consider the motion of an air parcel relative to that of the anomaly. The thermal anomaly shown in Fig. 3 rotates at a rate which is slower than the time scale associated with the motion of a parcel advected by the vortex flow. Therefore parcels of air move cyclonically through the thermal anomaly, and
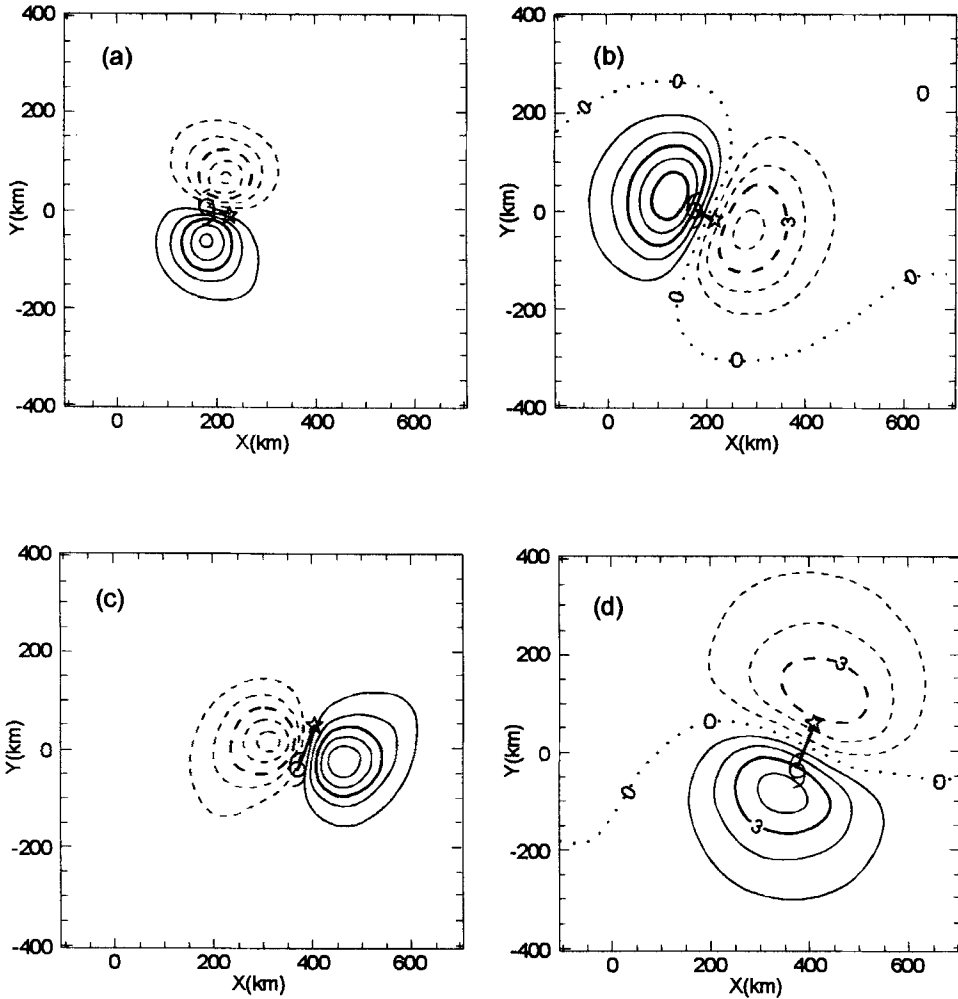
Figure 5.   Horizontal cross-sections at $z = 5$ km. (a) Vertical velocity at 24 hours, contour interval is 10 cm s^{-1}. (b) Potential-temperature perturbation at 24 hours, contour interval is 1 K. (c) Vertical velocity at 48 hours, contour interval is 5 cm s^{-1}. (d) Potential-temperature perturbation at 48 hours, contour interval is 1 K. In all figures the position of minimum geopotential at 1 km is marked by a cyclone symbol and that at 9 km by a star.

the pattern of vertical motion is that shown in Fig. 4(c). The 90° phase shift between the vertical velocity and potential-temperature perturbation can be seen in Fig. 3, and in the semi-balanced simulations shown in RA.

After the initial period of adjustment over the first 6 hours, the relationship between the tilt of the vortex and the orientation of the temperature anomaly and vertical velocity remains essentially constant. This is illustrated in Fig. 5, which shows the vertical velocity and potential-temperature perturbation at 24 and 48 hours. The vortex centre at $z = 1$ km is marked by a tropical cyclone symbol and that at $z = 9$ km by a star. The potential-temperature anomaly is maximum in the plane in which the vortex is tilted. The vertical velocity maximum lies perpendicular to this plane. Since the vortex tilt rotates with time, the vertical velocity and potential-temperature anomaly also rotate with time. Thus the expected relationship between the vertical velocity and environmental shear (the shear
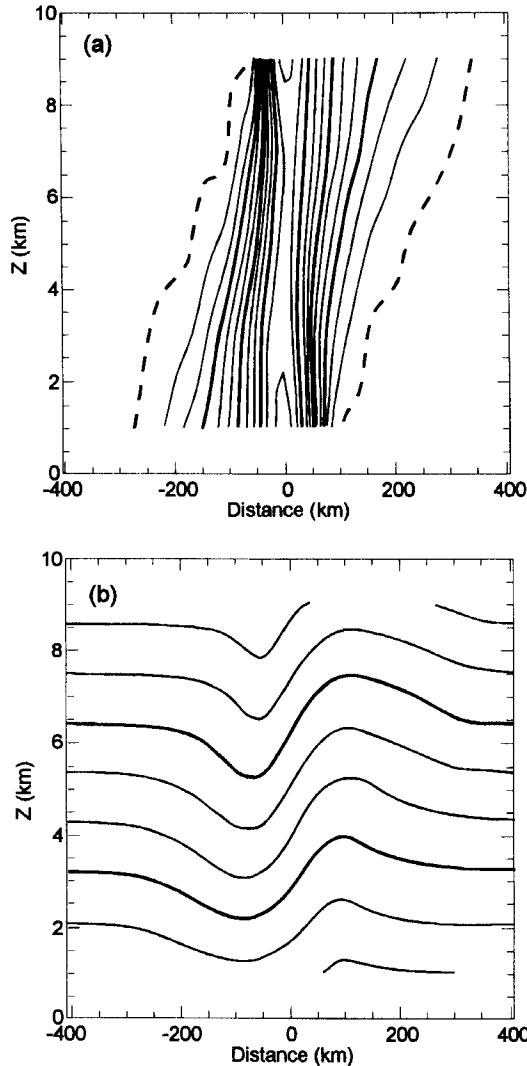
Figure 6. Vertical cross-sections parallel to the direction of tilt at 24 hours. The location of the cross-section is shown in Fig. 2(c). Variables are plotted from $z = 1$ km to $z = 9$ km (the lowest and highest potential-temperature levels on the staggered grid). (a) The density-weighted potential vorticity with contour interval of 0.5×10^{-6} m^{-1}s^{-1} K. (b) Potential temperature with contour interval of 5 K.

vector pointing to ascending motion) is only seen at the beginning of the model run. This constant relationship between the direction of tilt and the potential-temperature perturbation is consistent with the assumption that the model flow is balanced. Figures 6(a) and (b) show vertical cross-sections of the potential vorticity and the isentropes after 24 hours in the plane where the vertical tilt is maximum. The position of the cross-section is shown in Fig. 2(c). The isentropes are similar to those associated with the tilted potential-vorticity anomaly in RA.

The magnitude of the vertical velocity varies with time. As shown in Fig. 7 it increases to a maximum at around 24 hours and then decreases gradually. The vertical tilt increases steadily throughout the time period shown in Fig. 7. From the mechanism of Fig. 4(b) the early increase in vertical velocity can be attributed to the increasing vertical tilt and

the need for an associated thermal anomaly. The maximum amplitude of the potential-temperature perturbation is also shown in Fig. 7. It increases significantly over the first 24 hours and then slowly declines. The decrease in the vertical velocity occurs as the vortex itself weakens, as characterized by the curve of maximum relative vorticity. The decrease in the vertical component of relative vorticity is due to both the tilting of the vortex away from the vertical and to the diffusive terms in the model. If the vortex is weaker, the balanced thermal perturbation will be smaller for a given tilt. This would account for the thermal perturbation remaining relatively constant in amplitude while the vertical tilt increases.
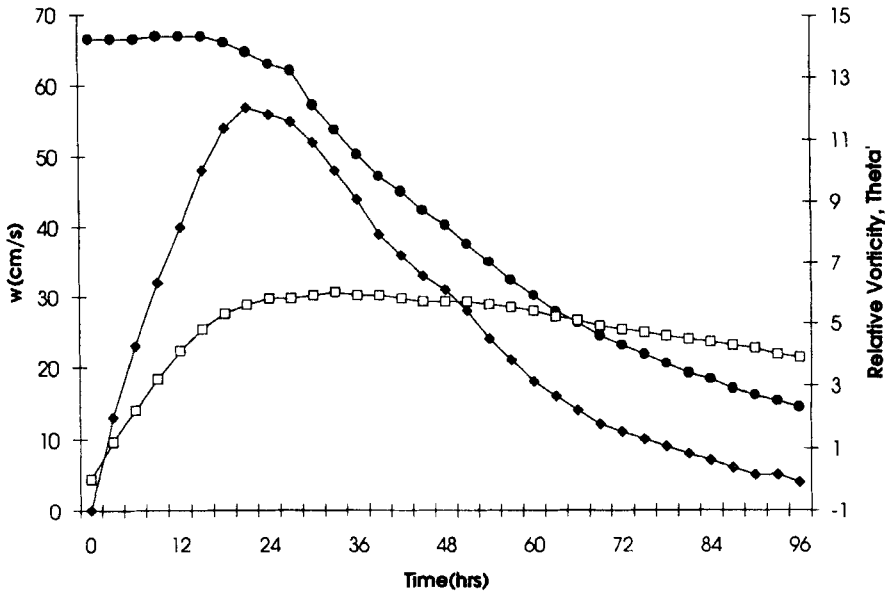
Figure 7.   Graph showing the maximum vertical velocity (diamond), maximum relative vorticity (circle) and maximum potential-temperature perturbation (square) at 3-hourly intervals. The relative vorticity is in units of $10^{-4}s^{-1}$.

In a balanced model the structure of the potential-temperature field is determined by the potential-vorticity structure. Hence if the tilted potential-vorticity anomaly rotates with time, the thermal anomaly automatically rotates with it. However, in these primitive-equation calculations, the relationship between the direction of tilt and the orientation of the potential-temperature anomaly depends on the relative magnitudes of the horizontal and vertical advection of the anomaly. The horizontal vortex flow will tend to rotate the thermal anomaly cyclonically, whereas the vertical advection of the environmental potential temperature tends to rotate the anomaly anticyclonically. This can be seen by referring to Fig. 4(c). In the region where descent takes place the potential-temperature anomaly will increase in amplitude, because of vertical advection. In the ascent region the potential-temperature anomaly will decrease. The vertical velocity required to counteract the horizontal advection will decrease as the strength of the vortex decreases, so that the decreasing vertical velocity seen in Fig. 7 is consistent with the maintenance of the thermal anomaly.

The vertical cross-section of the potential vorticity at 24 hours (Fig. 6(a)) shows that the inner-core region is not as strongly tilted as the outer regions of the vortex. The potential-vorticity maximum at the top is located almost directly above that at the surface. This feature can also be seen in Fig. 2(c), where at 24 hours the position of maximum potential vorticity at both upper- and lower-levels has been shifted off-centre, so that
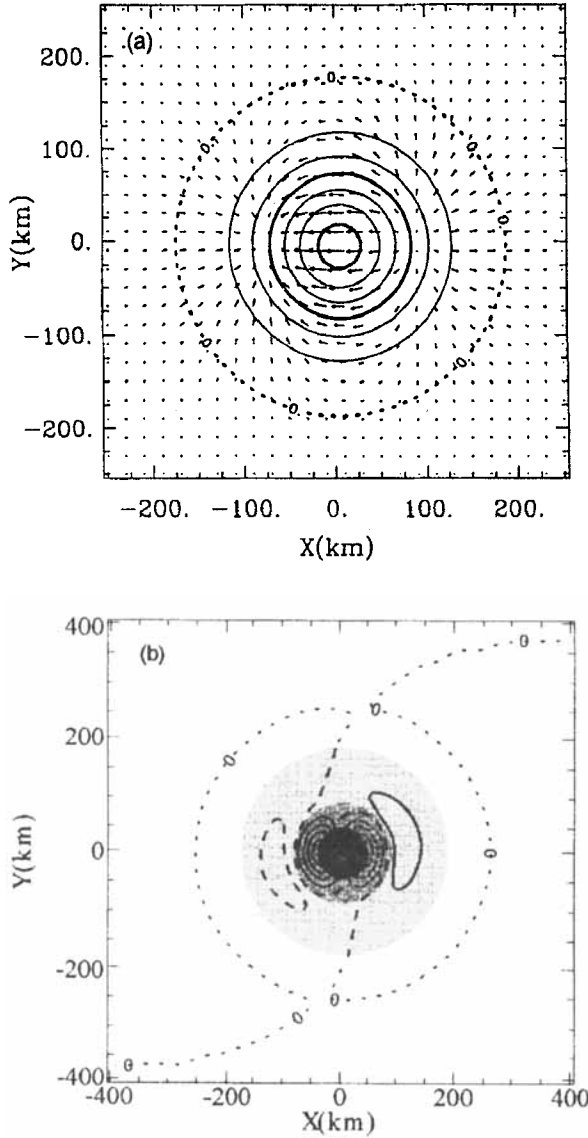
Figure 8. Horizontal cross-sections after 30 min at $z = 1$ km. (a) Divergent winds (maximum arow is 0.9 m s^{-1}) with contours of potential vorticity (contour interval is 1×10^{-6}m^{-1}s^{-1} K). (b) Contours of the tendency due to horizontal advection of potential vorticity by the divergent wind. Shaded area shows the region of positive potential vorticity.

the vortex is no longer axisymmetric. The explanation for this strong asymmetry can be found in the interaction between the vertical circulation and the initially symmetric vortex. The vertical circulation at the beginning of the model run has descent to the east of the vortex centre and ascent to the west. In order to satisfy the continuity equation, divergent horizontal winds are required, which are easterly at the surface and westerly at the upper boundary. The divergent horizontal wind after 30 minutes is shown by the vectors in Fig. 8(a). The contours are the potential vorticity. From this figure it can be seen that the divergent wind at the surface advects the potential-vorticity anomaly westwards. The converse is true at upper levels. Thus at first glance it appears that the advection by the

divergent circulation opposes the advection by the environmental shear flow. However, close inspection of Fig. 8(a) reveals that the divergent flow is not spatially uniform. The easterly flow is strongest at the vortex centre and decreases in amplitude as the radius increases. At a radius of about 100 km the divergent flow is zero, and for larger radii it is westerly and considerably weaker than at the vortex centre. The potential-vorticity tendency due to advection by this divergent flow is shown by the contours in Fig. 8(b). The shaded region shows the potential-vorticity anomaly. The tendency has a wavenumber-one component, which changes sign for radius larger than 100 km. The effect of this tendency will be to shift the position of maximum potential vorticity westwards relative to the outer potential-vorticity anomaly. Thus the vortex loses the initial axisymmetry. At upper levels the same effect is observed, but the position of the potential-vorticity maximum is shifted eastwards relative to the outer circulation. This is responsible for the inner core having a smaller vertical tilt than the larger scale anomaly.

During the later stages of the model run the vortex tilt, as defined by the position of minimum geopotential perturbation at each level, is not uniform with height. The distance between the vortex centre at 1 km and that at 3 km is smaller than the corresponding distance between 3 km and 5 km, as seen in Fig. 1(a). The vortex centres at 7 km and 9 km are also close together. This results from the distortion of the vortex described above being a function of height. The divergent flow is strongest at the highest and lowest model level, and is close to zero at mid-levels. Thus the distortion is strongest at $z = 1$ km and $z = 9$ km, weaker at $z = 3$ km and $z = 7$ km, and is negligible at $z = 5$ km. Figures 2(e) and 2(f) show that the vortex centre at the surface is displaced to the northwest side of the potential-vorticity anomaly. Similarly, the vortex centre at 9 km is displaced to the southwest side of the upper-level potential-vorticity anomaly. Thus both the upper- and lower-level centres are displaced towards the mid-level centre. At $z = 3$ km and $z = 7$ km the centres are only slightly displaced towards the mid-level centre. Thus the tilt appears to be non-uniform with height. A consequence of the distortion is that the potential-vorticity structure resembles two separate anomalies, rather than a tilted vortex. This can be seen in Fig. 9, which shows vertical cross-sections of the density-weighted potential vorticity and the potential-temperature perturbation at 96 hours. The position of the cross-section is marked in Fig. 2(f). The upper-level anomaly is cold core and the lower-level anomaly warm core, as seen in Fig. 9(b).

The role played by the vertical circulation was discussed by WHL in terms of relative vorticity. The important contributions to the relative-vorticity budget are the advection by the divergent circulation and the stretching term due to horizontal divergence. WHL propose that the stretching and vertical advection terms in the relative-vorticity equation reduce the vertical tilt of the vortex by opposing the advective tendency due to the background shear flow. The results described here show that this mechanism can reduce the vertical tilt only in the inner core region. It occurs on too small a scale to explain the motion of the vortex as a whole relative to the environmental shear flow. This is illustrated in Fig. 10(a), which shows the relative-vorticity tendency due to stretching after 30 minutes, and Fig. 10(b), which shows the tendency due to advection by the environmental flow at the same level ($z = 1$ km). The tendency due to vertical advection is not shown, as it is two orders of magnitude smaller than that due to stretching at this level. In both figures the relative vorticity is shaded. The stretching tendency has larger amplitude than the tendency due to advection by the environmental flow and the orientation of the two tendency terms is such that they oppose each other. However, the horizontal scale of the stretching tendency is considerably smaller than that of the advective tendency. Hence this tendency acts to deform the vortex, rather than to oppose the advective tendency due to the environmental shear flow.
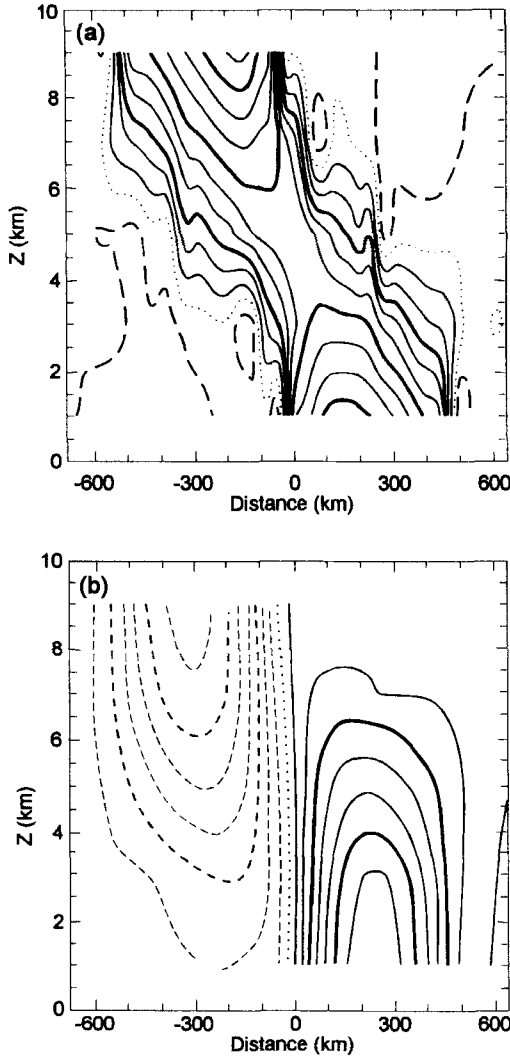
Figure 9. Vertical cross-sections parallel to the direction of tilt at 96 hours. The location of the cross-section is shown in Fig. 2(f). Variables are plotted from $z = 1$ km to $z = 9$ km (the lowest and highest potential-temperature levels on the staggered grid). (a) Density-weighted potential vorticity with contour interval of 0.1×10^{-6} m^{-1}s^{-1} K. (b) Potential-temperature perturbation, contour interval is 0.5 K.

The distortion of the symmetric vortex results in a horizontal separation between the vorticity centre, defined as the position of maximum relative vorticity, and the centre of circulation, defined as the location at which the non-divergent flow is zero. This can be seen in Fig. 11, which shows contours of the relative vorticity at 24 hours for $z = 1$ km and $z = 9$ km. The non-divergent wind field is shown by arrows. At $z = 1$ km the centre of circulation is located to the west of the vorticity centre. At $z = 9$ km the centre of circulation is to the east of the vorticity centre. Thus the non-divergent flow at the vorticity centre is no longer zero, as is the case for an axisymmetric vortex. There is a southerly component at the vorticity centre at $z = 1$ km and a northerly component at $z = 9$ km. This leads to northwards motion of the lower-level relative-vorticity maximum and southwards motion of the upper-level maximum. This motion is part of a cyclonic rotation of the vorticity
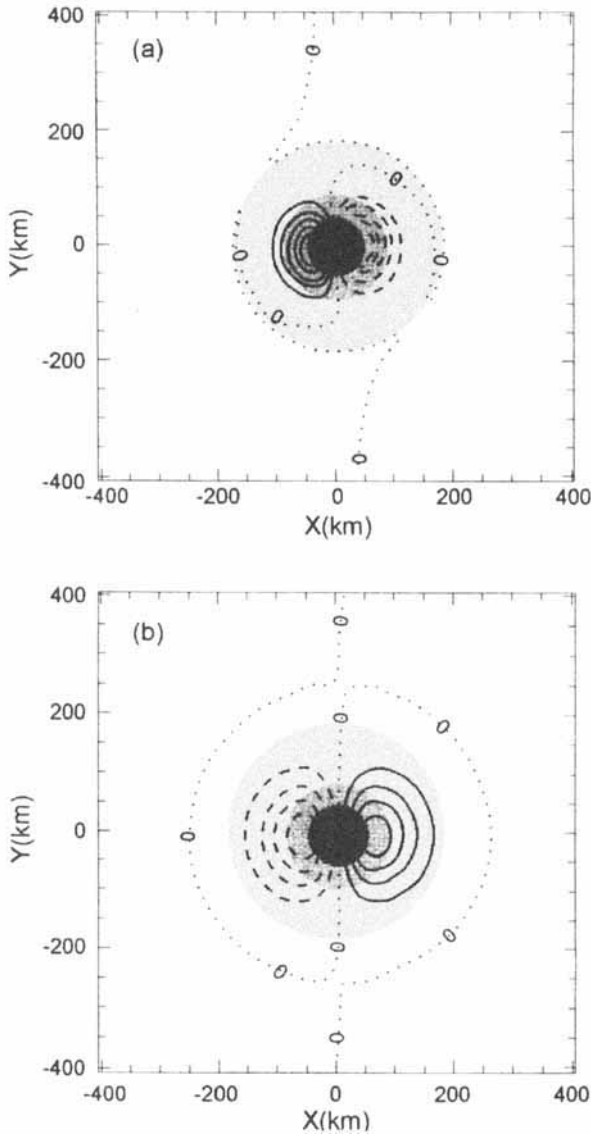
Figure 10. Horizontal cross-sections after 30 min at $z = 1$ km. (a) Contours of the stretching tendency in the vorticity equation, contour interval is $2.5 \times 10^{-7} s^{-2}$. Shaded region shows positive relative vorticity. (b) Contours of the vorticity tendency due to advection by the environmental flow, contour interval is $1 \times 10^{-8} s^{-2}$. Shaded region as in (a).

centre, within the larger-scale vorticity anomaly. In contrast, the downward projection of the upper-level anomaly leads to northerly flow across the lower-level anomaly, and the upward projection of the lower-level anomaly leads to southerly flow across the upper-level anomaly. Hence the instantaneous motion of the vorticity or potential-vorticity centre is in the opposite direction of that of the large-scale anomaly.

Figure 11 shows that after 24 hours the vorticity centre has rotated through 180° about the centre of the large-scale anomaly. As described previously, the surface vorticity centre is initially displaced westwards by the action of the divergent flow. The subsequent cyclonic rotation of the vorticity centre within the large-scale anomaly results in the eastward
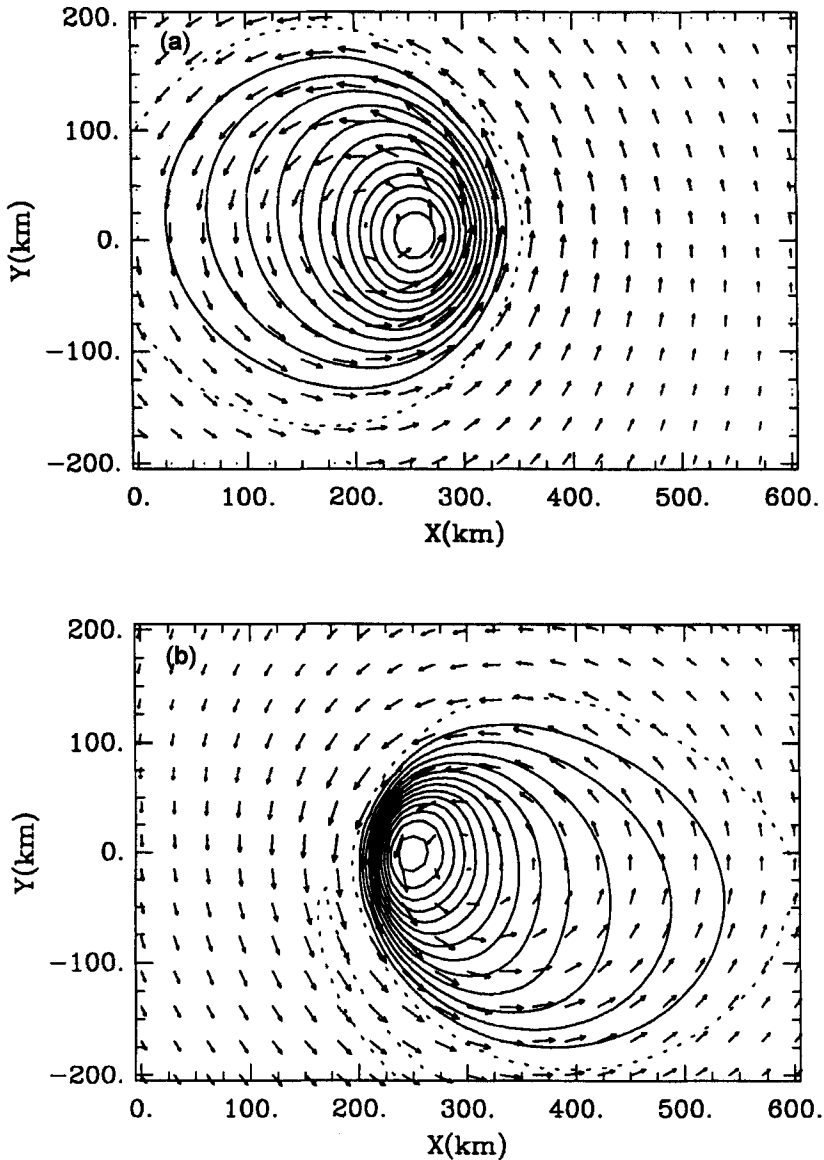
Figure 11.   Horizontal cross-sections at 24 hours. Contours of relative vorticity, contour interval is $1 \times 10^{-4} \text{s}^{-1}$. Arrows indicate non-divergent wind. (a) $z = 1$ km, maximum vector is 46 m s^{-1}. (b) $z = 9$ km, maximum vector is 51 m s^{-1}.

displacement seen in Fig. 11(a). At upper levels the initial displacement of the vorticity centre was to the east. After 24 hours the vorticity centre has rotated cyclonically to give a westward displacement of the position of maximum relative vorticity relative to the large-scale anomaly (Fig.11(b)).

     We could consider the vortex shown in Fig. 11(a) to consist of two vortices of different size, where the centre of the small-scale vortex is displaced to the east of the centre of the large-scale vortex. The behaviour described above can be attributed to the advection of the small-scale vortex by the flow associated with the large-scale vortex. The small-scale vortex will also influence the motion of the large-scale vortex. At the surface, the centre of

the large-scale vortex is to the west of that of the small-scale vortex. Thus the flow across the centre of the large-scale vortex due to the small-scale vortex is northerly, resulting in a southwards motion of the large-scale vortex. This effect can be seen in Fig. 11(a) as the cross-contour flow to the west of the centre of circulation, which advects the outer region of the vortex southwards, as does the flow associated with the downward projection of the upper-level vortex. This suggests that the mutual rotation will be reinforced by the distortion of the symmetric vortex which results from the action of the vertical circulation. The distortion also gives rise to a stronger potential-vorticity anomaly in the region where the upper- and lower-level vortices overlap. This will enhance the effect of one anomaly on the other, and so strengthen the mutual rotation which reduces the destructive effect of the shear on the vortex. These effects are considered to be complementary to the mechanism discussed in section 3, but are not expected to dominate, for reasons which are discussed in the next section.

The wind fields seen in Fig. 11 are mainly associated with the potential-vorticity anomaly on the level shown. They may contain also a component from the upward or downward projection of the tilted potential-vorticity anomaly. The magnitude of this component is small, since the wind field associated with a potential-vorticity anomaly decays with height. In order to observe the wind field associated with the vortex tilt it would be necessary to subtract the flow associated with the potential vorticity at the level shown from the total flow. The technique used in barotropic studies, where an axisymmetric vortex centred on the position of maximum relative vorticity is subtracted from the total vorticity, has been applied to this data. The resulting asymmetry field is dominated by a strong wavenumber-one asymmetry, whose horizontal scale is smaller than that of the symmetric vortex. It can be shown that this asymmetry develops due to the distortion of the symmetric vortex by the divergent circulation. A more sophisticated analysis would be required to isolate the weaker asymmetry associated with the tilt of the vortex.

The amplitude of the asymmetry due to the distortion of the vortex is a maximum at the radius of maximum wind, so that the structure of the asymmetry resembles that due to a misplaced centre. However, these asymmetries should not be confused with those due to a misplaced centre since they arise from the physical mechanism described above. The divergent flow is a maximum at the surface and upper-levels and has a small amplitude at mid-levels. This results in the amplitude of wavenumber-one asymmetry being small at mid-levels also. Both the asymmetry and the divergent wind change sign with height.

The separation between the centre of circulation and the centre of vorticity or potential vorticity leads us to question how the vortex centre should be defined. An appropriate dynamical definition might be considered to be the position of maximum potential vorticity. However, this is strongly influenced by the mesoscale structure of the vortex, which arises due to the action of the vertical circulation. The relationship between the potential vorticity and the geopotential is such that the geopotential appears as a smoothed version of the potential vorticity (Hoskins et al. 1985). Thus the position of minimum geopotential is not as strongly influenced by small-scale effects, such as the distortion of the vortex. Hence using the position of minimum perturbation geopotential to define the vortex centre gives a clearer picture of the overall behaviour of the vortex, especially of the development of the vertical tilt. The difference between the potential vorticity centre and the geopotential centre can be seen in Figs. 1(b) and 1(c). After 48 hours the vortex tilt appears larger if the geopotential is used to define the centre. The angle of tilt differs also between the two cases. In Fig. 2(d) it can be seen that using the geopotential to define the centre underestimates the vertical tilt also, although not by as much as when the potential vorticity defines the centre. The problem of the most suitable definition of the vortex centre in the presence of vertical shear requires further study.

5. VARYING THE PENETRATION DEPTH AND OTHER PARAMETERS

In this section results are presented from experiments where the various parameters used for the model run described in the previous two sections (referred to hereafter as the standard run) are altered. The minimum perturbation geopotential is used to define the vortex centre in all of the tracks shown in this section. The behaviour as described above might be expected to alter if the vertical shear increases, since this affects the magnitude of vertical tilt. The magnitude of the vertical penetration depends on the Coriolis parameter, the static stability, the horizontal length scale, and the vortex strength. The influence of these parameters is tested by comparing model runs of 36 hour duration. The parameters used are given in Tables 1 and 2. The rotation rate referred to below is defined as the rate at which the upper- and lower-level centres rotate about the position of the mid-level centre.

Figure 12 shows the vortex tracks for two cases with stronger vertical shear than
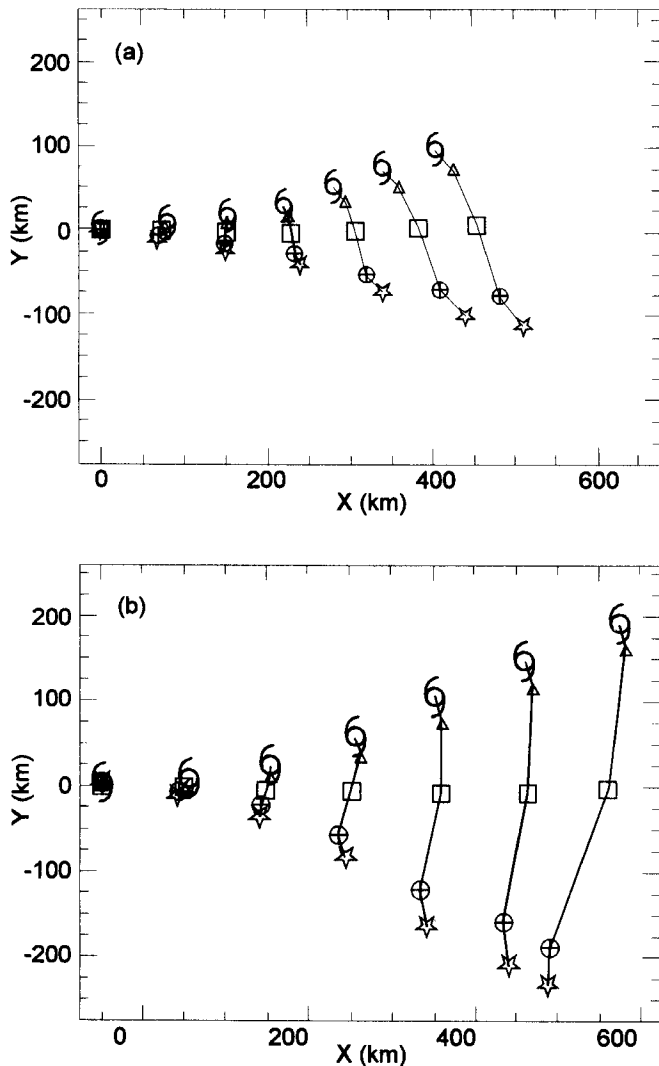
Figure 12.   Vortex tracks with parameters as in standard run except (a) $U_0 = 6 \text{ m s}^{-1}$, $U_z = -6 \times 10^{-4}\text{s}^{-1}$, (b) $U_0 = 8 \text{ m s}^{-1}$, $U_z = -8 \times 10^{-4}\text{s}^{-1}$. Symbols are as in Fig. 2.

that used in the standard run (6 m s^{-1}/10 km and 8 m s^{-1}/10 km). All other parameters are identical to those of the standard run. These tracks should be compared with the first 36 hours shown in Fig. 1(b). As the shear increases, the vertical tilt of the vortex increases and the rotation rate decreases. Neither case exhibits rotation through 180°. In contrast to the standard run, the surface centre moves northwards and the upper-level centre southwards. After an initial period of rotation the direction of the tilt does not change significantly, but the magnitude steadily increases. The same behaviour was observed for the standard run after 72 hours. The time taken to reach this constant tilt, and the angle of the tilt, depends on the magnitude of the shear. Experiments were performed with weaker shear than that of the standard run. In all cases the vortex tilt increased with time, although for weaker shear a longer integration time was required in order to observe the increase of the tilt. The weakest shear used was 0.5 m s^{-1}/10 km.
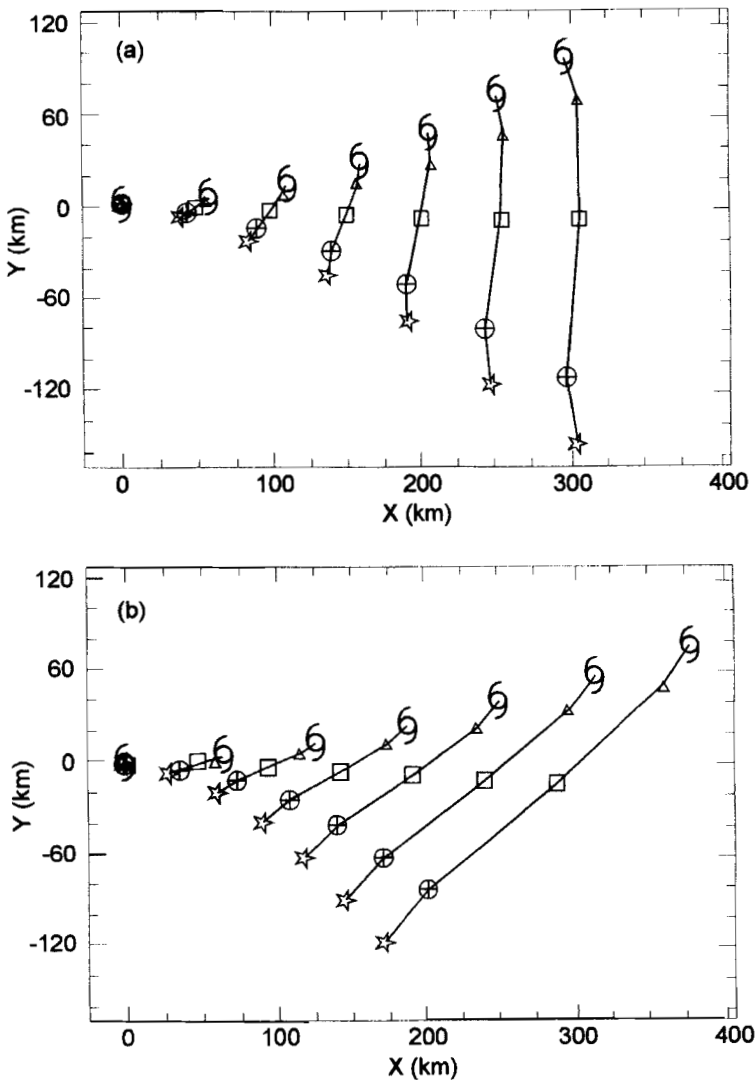
Figure 13.   Vortex tracks as in standard run except (a) $v_{max} = 30$ m s^{-1}, (b) $v_{max} = 20$ m s^{-1}.

In Fig. 13 the effect of varying the strength of the vortex whilst keeping all other parameters as in the standard run is illustrated. The maximum tangential wind is reduced by using a smaller value of v_0 in Eq. (1). The radial profile remains unchanged. Figure 13(a) shows the track of a vortex with a maximum tangential wind speed of 30 m s^{-1}. The initial behaviour is as in Fig. 1(b). However, the rotation is slower, with a N–S tilt being reached after 24 hours for the weaker vortex compared to 12 hours in the standard run. The direction of tilt remains N–S up to 36 hours, whilst the magnitude of the tilt increases. Figure 13(b) shows the same experiment with a maximum tangential wind of 20 m s^{-1}. In this case the rotation is slower and the vertical tilt larger than in Fig. 13(a). The direction of tilt remains approximately constant after 12 hours, with a NE–SW orientation. In neither case is the rotation sufficient to reach the stage where the tilt is opposite to that expected from the vertical shear. The vortex strength enters the problem in two ways. As previously discussed, the penetration depth depends on the strength of the anomaly. Hence for a weaker potential-vorticity anomaly the flow associated with that anomaly decays more strongly with height. A second effect is that the flow at the level of the anomaly is weaker, and therefore the flow due to the downward penetration is weaker. This results in reduced advection at a given level due to anomalies at other levels.

The consequences of altering either the Coriolis parameter or the static stability are shown in Fig. 14. In Fig. 14(a) the track from a model run with the 30 m s^{-1} vortex and a static stability of 1×10^{-4} s^{-2} can be seen. This is identical to the run shown in Fig. 13(a) except for the reduced static stability. Comparison of Figs. 13(a) and 14(a) shows that the vertical tilt is considerably smaller for lower static stability and the rotation rate larger. This can be attributed to the increased penetration depth due to the decrease in static stability. A similar effect is observed in Fig. 14(b) where the parameters are again those used for Fig. 13(a), except that the f-plane is situated at 20°N. This will also increase the penetration depth. From the tracks shown it appears that in both cases the rotation will continue as in the standard run, so that the lower-level vortex centre eventually moves southwards and the upper-level vortex centre moves northwards.

The problem of finding an appropriate form for the penetration depth was discussed in section 3. An example was quoted using average values of relative vorticity and tangential wind and assuming a length scale of 360 km. If the same expression is used to calculate the penetration depths for the runs shown in Figs. 13(a), 14(a) and 14(b), the respective penetration depths are 10.7 km, 13.1 km and 11 km respectively. This would suggest that the change in Coriolis parameter would not have a large effect, in contrast to the results presented above. It would appear that this definition of the penetration depth is not wholly satisfactory.

Figure 14(c) shows the track of a vortex with the same parameters as the standard run, but for $f = 0$. In this case rotation is observed also. This is consistent with including the strength of the vortex and a local Coriolis parameter in the penetration depth in a manner described in section 3. Use of a quasi-geostrophic penetration depth, which is zero for this case, would imply that no rotation would occur. As in the previous cases, the vortex initially rotates, then the rotation slows to give a fairly constant tilt. The final tilt is such that the surface vortex is significantly retarded and the upper-level vortex accelerated by their mutual interaction.

Another factor which should influence the penetration depth is the horizontal length scale of the anomaly. This is tested by using the vortex profile given in Eq. (2) with a radius of maximum wind at 150 km and a radius of gale force wind at 470 km. The other parameters used are as for Fig. 12(a) (shear of 6 m s^{-1}/10 km). The track is shown in Fig. 15(a). The broader vortex is much less susceptible to the action of the vertical shear. The vertical tilt is smaller and the rotation rate higher than for the smaller-scale anomaly.
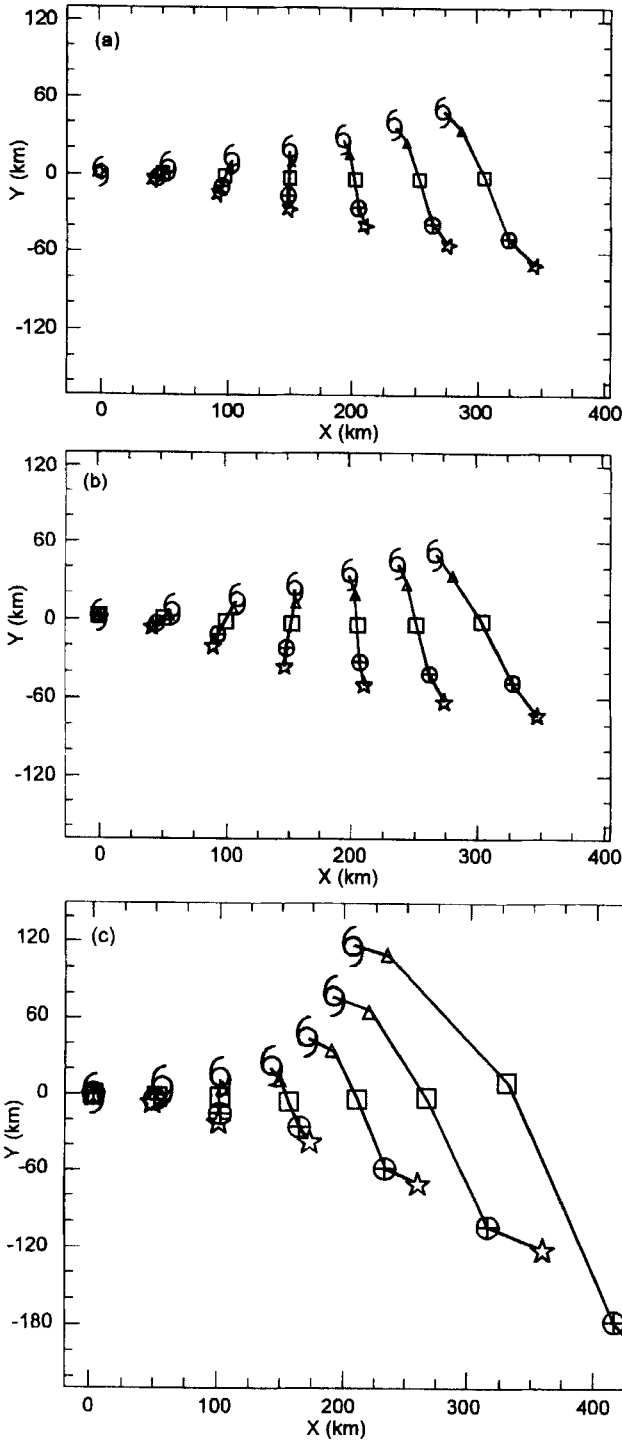
Figure 14.   (a) As in Fig. 13(a) but $N^2 = 1 \times 10^{-4} \text{s}^{-2}$. (b) As in Fig. 13(a) but f-plane at 20°N. (c) As in standard run but $f = 0$.
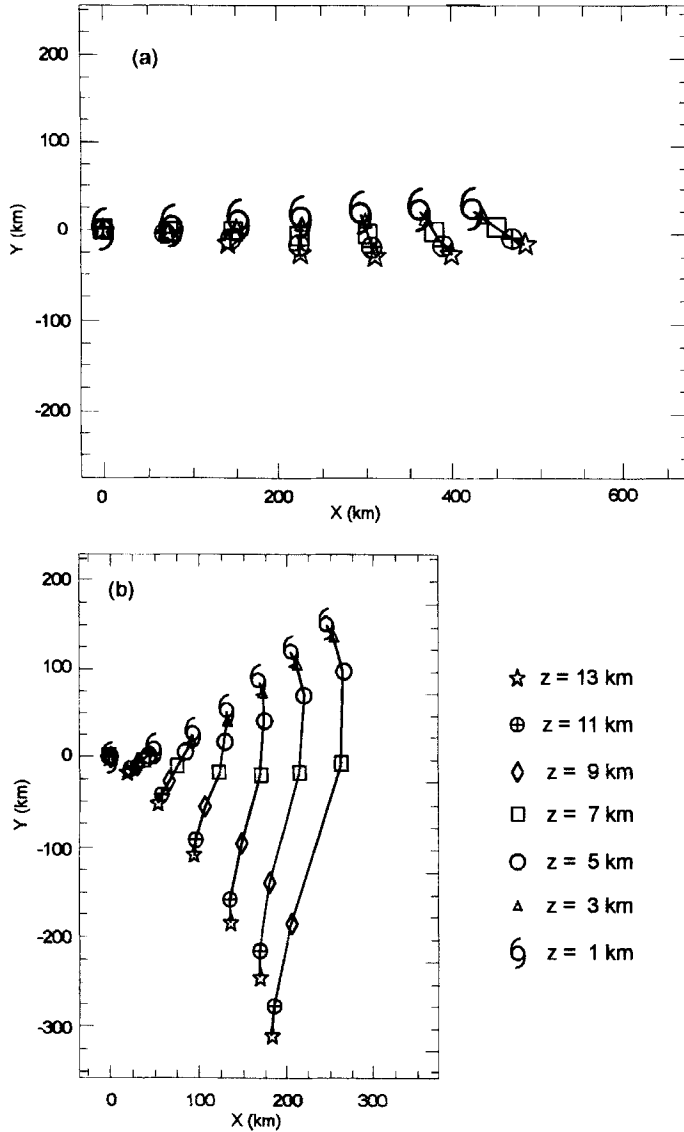
Figure 15.   Vortex tracks as in standard run but (a) broader profile given by Eq. (2) is used. Symbols are as in Fig. 1. (b) vortex height is 14 km. Symbols are given in key.

It appears that in this case the rotation will be sufficient for the surface centre to move southwards.

Changing the height of the vortex also has an impact on the susceptibility to shear. Figure 15(b) shows a calculation identical to that in section 3, except for the height of the vortex which is 14 km. The vertical tilt of the vortex is much larger than for a 10 km high vortex. This would be expected since the difference between the environmental flow at the surface and the upper boundary is larger in this case.

If the direction of shear is reversed the behaviour is comparable to that described previously. In this case the initial motion of the surface centre is southwards and that of the upper-level centre is northwards. The other features described in section 4 are seen, with

ascent initially on the downshear side of the vortex, the development of the temperature anomaly and the constant phase relation between the tilt of the vortex, the vertical velocity field, and the temperature anomaly.

It is interesting to consider the relationship between the vertical circulation and the vertical tilt for the different runs. We have presented several cases where the shear was held constant and other parameters altered. It has been shown that changing certain parameters, for example increasing the Coriolis parameter, results in a smaller vertical tilt for the same magnitude of shear. We infer from this that the mechanism which opposes the tilt acts more strongly in the case where the tilt is smaller. WHL suggest that the vertical circulation acts against the vertical shear to reduce the vertical tilt. Thus we would expect to observe larger vertical velocity in the aforementioned case where the tilt is smaller. However, the vertical velocity was smaller in this case. This is not consistent with the vertical circulation opposing the vertical shear. It is consistent with the idea that the vertical circulation acts so as to maintain balance, since if the vertical tilt is smaller, the required thermal anomaly is smaller. Therefore the vertical circulation required to produce this anomaly does not need to be as large as in a case with larger vertical tilt. One case where the vertical velocity was comparable for different vertical tilts was that where the static stability was reduced. However, the thermal anomaly in this case had smaller amplitude for the case with smaller tilt. Since the static stability was reduced, a larger vertical velocity is required to produce the same amplitude potential-temperature anomaly by vertical advection of the environmental temperature field. The variation in vertical velocity when either the Coriolis parameter is increased or the static stability is reduced suggests that the mechanism for the vertical circulation shown in Fig. 4(a) (vortex motion along the background isentropes) is not as important as that in Fig. 4(b). The increase of Coriolis parameter or decrease in static stability leads to the isentropes being more strongly tilted. The mechanism of Fig. 4(a) would imply that the vertical circulation should be stronger, which is not the case.

The dependence of the rotation rate on the penetration depth is in accordance with the explanation given in section 3 for the occurrence of this rotation. An increase in the penetration depth resulted in a higher rotation rate and a decrease in penetration depth in a lower rotation rate. It was suggested in section 4 that the distortion of the symmetric vortex by the vertical circulation could result in a similar rotation. However, the speed of rotation resulting from this distortion depends on the strength of the vertical circulation and not directly on the penetration depth. Therefore we propose that the rotation arises primarily from the vertical interaction of the upper- and lower-level anomalies.

6.   SUMMARY AND DISCUSSION

This paper has described the behaviour of initially-barotropic vortices in an environmental flow with vertical shear. The study was aimed at understanding some of the mechanisms responsible for the behaviour of tropical cyclones in vertical shear. However, the results are applicable to any other situation of a strong vortex in an environment with relatively weak vertical shear. The initial effect of the environmental flow is to tilt the vortex from the vertical. As soon as the vortex starts to tilt, the upper- and lower-level centres start to rotate cyclonically about the mid-level centre. This is analogous to the barotropic two-vortex problem, but in the present case the vortex at each level is advected by the circulation due to the vertical penetration of the tilted vortex.

The rotatory behaviour of the vortex provides a mechanism which opposes the destructive action of the vertical shear. The flow associated with the vertical penetration of the tilted potential-vorticity anomaly is itself vertically sheared. The direction of this shear in the east–west plane depends on the north–south tilt of the vortex. The initial response

of a vortex to environmental vertical shear results in the vertically-sheared flow associated with the tilted vortex having the opposite sign to the environmental shear. This acts to reduce the effect of the vertical shear, unless the direction of tilt rotates through 180°. If this takes place, the vertical shear associated with the tilted vortex and the environmental vertical shear have the same sign. A second contribution of the rotation towards reducing the vertical shear occurs if the direction of tilt rotates through an angle greater than 90°. Such a rotation leads to a vertical tilt in the E–W plane which is opposite to that expected from the direction of shear. The subsequent action of the vertical shear tends to reduce the vertical tilt, rather than increasing it.

The susceptibility of the vortex to vertical shear was shown to depend on the penetration depth. The penetration depth is increased by increasing the Coriolis parameter, decreasing the static stability, and increasing the strength or size of the vortex. Increasing the penetration depth resulted in the vortex having a smaller vertical tilt after a given period of time and led to an increase in the rotation rate. The highest rotation rate was observed in the early stages of a given model run. The rotation rate decreased gradually with time, so that the vortex eventually reached a constant direction of tilt. The magnitude of the tilt continued to increase with time. The final tilt that was reached and the time taken to reach it varied for the different penetration depths. In some cases the final tilt was such that the vortex centre at the surface moved southwards, and in other cases the surface centre moved northwards. Previous authors have assumed that the interaction between a cyclonic upper-level vortex and a cyclonic lower-level vortex will result in motion to the right of the vertical shear. The calculations described here show that this is not necessarily the case. The surface centre may move either to the right or to the left of the vertical shear, depending on the parameters which determine the penetration depth.

The development of the vertical circulation has been studied in detail. The initial pattern of vertical circulation was a wavenumber-one couplet, with ascent on the downshear side of the vortex. This rotated with time, anticyclonically at first and later cyclonically. A potential-temperature anomaly developed in association with the vertical circulation. After an initial adjustment period of less than 6 hours, the relationship between the direction of vortex tilt and the phases of the potential temperature and vertical velocity fields remained constant. The development of the vertical circulation can be associated with the maintenance of balance. Once the potential-vorticity anomaly is tilted by the vertical circulation, a thermal anomaly is required for the flow to be balanced. The vertical circulation acts to produce this thermal anomaly by vertical advection of the stably-stratified fluid. As the potential-temperature anomaly develops, it is advected by the cyclonic vortex circulation. The phase shift between the vertical velocity and the potential-temperature perturbation means that the vertical advection of environmental potential temperature opposes the horizontal advection of the thermal anomaly by the vortex flow. This allows the thermal anomaly to remain in phase with the tilted vortex.

The vertical circulation is seen to be important in the maintenance of balance. It does not play the role envisaged by WHL in opposing the advection by the environmental shear flow. In the calculations described here, the mechanism described by WHL operates on a smaller scale than that required to reduce the vertical tilt of the vortex as a whole. It acts to distort the symmetric vortex, such that the inner core of the vortex has a smaller vertical tilt than the outer region. A consequence of this distortion is that a strong wavenumber-one asymmetry develops in the vortex core. This has a similar appearance to the asymmetry associated with a misplacement of the vortex centre, but arises through a different mechanism. Since the asymmetry changes sign with height it would not be possible to remove it from all levels by choosing a different centre.

The study of adiabatic initially barotropic vortices presented here has enabled us to

isolate one of the mechanisms which influence the behaviour of hurricane-like vortices in vertical shear. The use of an initially barotropic vortex was particularly useful in examining the potential-temperature perturbation, since the vortex itself has no thermal structure. This assisted us in our understanding of the role of the vertical circulation. However, it is possible that some of the details described here may change if the initial vortex more closely resembles a tropical cyclone. This problem is addressed in a future paper.

REFERENCES

Arakawa, A. and Lamb, V. R.	1977	Computational design of the basic processes of the UCLA general circulation model. *Methods Comput. Phys.*, **17**, 173–265.
Charney, J. G.	1955	The use of primitive equations of motion in numerical prediction. *Tellus*, **7**, 22–26.
Chan, J. C. and Williams, R. T.	1987	Analytical and numerical studies of the beta-effect in tropical cyclone motion. Part I: Zero mean flow. *J. Atmos. Sci.*, **44**, 1257–1265
Davis, C. A.	1992	Piecewise potential vorticity inversion. *J. Atmos. Sci.*, **49**, 1397–1411
Eady, E. T.	1949	Long waves and cyclone waves. *Tellus*, **1**, 33–52
Fiorino, M. and Elsberry, R. L.	1989	Some aspects of vortex structure related to tropical cyclone motion. *J. Atmos. Sci.*, **46**, 975–990.
Flatau, M., Schubert, W. H. and Stevens, D. E.	1994	The role of baroclinic processes in tropical cyclone motion. Part I: The influence of vertical tilt. *J. Atmos. Sci.*, **51**, 2589–2601
Gent, P. R. and McWilliams, J. C.	1983	Regimes of validity for balanced models. *Dyn. Atmos. and Oceans*, **7**, 167–183.
Hoskins, B. J.	1971	Atmospheric frontogenesis models: some solutions. *Q. J. R. Meteorol. Soc.*, **97**, 139–153.
Hoskins, B. J., McIntyre, M. E. and Robertson, A. W.	1985	On the use and significance of isentropic potential vorticity maps. *Q. J. R. Meteorol. Soc.*, **111**, 877–946.
Jones, S. C. and Thorpe, A. J.	1992	The three-dimensional nature of 'symmetric' instability. *Q. J. R. Meteorol. Soc.*, **118**, 227–258
Lorenz, E. N.	1960	Energy and numerical weather prediction. *Tellus*, **12**, 364–373.
Madala, R. V. and Piacsek, S. A.	1975	Numerical simulation of asymmetric hurricanes of a β-plane with vertical shear. *Tellus*, **27**, 453–468.
McWilliams, J. C.	1985	A uniformly valid model spanning the regimes of geostrophic and isotropic, stratified turbulence: balanced turbulence. *J. Atmos. Sci.*, **42**, 1773–1774.
Polvani, L. M.	1991	Two-layer geostrophic vortex dynamics. Part 2. Alignment and two-layer V-states. *J. Fluid Mech.*, **225**, 241–270.
Raymond, D. J.	1992	Nonlinear balance and potential-vorticity thinking at large Rossby number. *Q. J. R. Meteorol. Soc.*, **118**, 987–1015.
Shapiro, L. J.	1992	Hurricane vortex motion and evolution in a three-layer model. *J. Atmos. Sci.*, **49**, 140–153.
Shapiro, L. J. and Montgomery, M. T.	1993	A three-dimensional balance theory for rapidly rotating vortices. *J. Atmos. Sci.*, **50**, 3322–3335.
Shapiro, L. J. and Ooyama, K. V.	1990	Barotropic vortex evolution on a beta-plane. *J. Atmos. Sci.*, **47**, 170–187.
Smith, R. K., Ulrich, W. and Dietachmeyer, G.	1990	A numerical study of tropical cyclone motion using a barotropic model. I: The role of vortex asymmetries. *Q. J. R. Meteorol. Soc.*, **116**, 337–362.

Wang, Y., Holland, G. J. and   1993   'Some baroclinic aspects of tropical cyclone motion'. Pp. 280–285
    Leslie, J. M.   in *Tropical Cyclone Disaster*. Eds. J. Lighthill, K. Emanuel,
                                                      G. Holland and Z. Zhemin. Peking University.

Wang, B. and Li, X.   1992   The beta drift of three-dimensional vortices: a numerical study.
                                                      Mon. Weather Rev., **120,** 579–593.

Wu, C.-C. and Emanuel, K. A.   1993   Interaction of a baroclinic vortex with background shear: applica-
                                                      tion to hurricane movement. *J. Atmos. Sci.*, **50,** 62–76.